Int. J. Electrochem. Sci., 13 **(2018)** 6958 – 6977, doi: 10.20964/2018.07.19

International Journal of ELECTROCHEMICAL SCIENCE
www.electrochemsci.org

Electrochemical and Quantum Chemical Studies of Adsorption and Corrosion Inhibition of Two New Schiff Bases on Carbon Steel in Hydrochloric Acid Media

Houria Debab [1], *Tahar Douadi* [1], *Djamel Daoud* [1,2,*], *Saifi Issaadi* [1], *Salah Chafaa* [1]

[1] Laboratoire d'Electrochimie des Matériaux Moléculaires et Complexes (LEMMC), Département de Génie des Procèdes, Faculté de Technologie, Université Ferhat ABBAS de Sétif-1, 19000 Sétif, Algeria

[2] Unité de Recherche Appliquée en Energies Renouvelables, URAER, Centre de Développement des Energies Renouvelables, CDER, 47133, Ghardaïa, Algeria

[*]E-mail: daoudkamal88@yahoo.fr.

Received: 23 January 2018 / *Accepted:* 15 March 2018 / *Published:* 5 June 2018

The inhibiting effect of two newly synthesized Schiff bases was investigated on the corrosion of carbon steel in 1M hydrochloric acid solution under various conditions by weight loss, impedance, and potentiodynamic polarization measurements. The Schiff bases used were 4,4'-bis (2-hydroxy-1-naphthaldehyde imine) diphenylether (L1) and 4,4'-bis(2-Hydroxy-1-naphthaldéhyde imine) diphenylmethane (L2). The inhibition efficiency of these compounds varied with concentration and immersion time. Potentiodynamic polarization study indicated that the tested compounds are mixed type (cathodic/anodic) inhibitors. Electrochemical impedance spectroscopy was also used to investigate the mechanism of corrosion inhibition, it showed that the charge transfer resistance (R_{ct}) increased and double layer capacitance (C_{dl}) decreased with an increase in the inhibitor concentration. The inhibition efficiency was found to increase with increasing inhibitor concentration. The adsorption of the inhibitor on the metal surface obeys Langmuir isotherm.

Keywords: Schiff base, Carbon steel, Corrosion inhibitor, EIS, Polarization, DFT.

1. INTRODUCTION

Compounds were synthesized from the condensation reactions product of an amine and ketone or aldehyde with a general formula of R_2C=NR–Schiff bases are well-known organic inhibitors [1,2]. The use of organic products type Schiff bases as corrosion inhibitors for carbon steel has expected a great importance in reason of their application in the prevention of corrosion under various aggressive environments [3,4]. Many research works shown that the inhibition efficiency of Schiff bases is much

greater than that of corresponding amines and aldehydes and attributed this to the presence of an –HC=N– group in the molecules which enriches the electron cloud [5–7]. Synthesis and characterization of Schiff bases are very important because of their potential applications and properties such as anticancer, anticonvulsant, antitumor, antifungal, antibacterial, antitubercular, antioxidant, antimalarial, anti-inflammatory, corrosion inhibitor, biological, anti- HIV and pesticidal properties [8]. Heterocyclic organic compounds containing nitrogen, sulphur or oxygen atoms are often used to protect metals from corrosion [9]. These atoms are the active sites for the process of adsorption on the metal surface. The adsorption process, and consequently the inhibition efficiency and even the inhibition mechanism depend on the electronic and structural characteristics of the inhibitor, the nature of the surface, the temperature and pressure of the reaction, the flow velocity as well as composition of the aggressive environment [10–13]. Theoretical chemistry has been used recently to explain the mechanism of corrosion inhibition, such as quantum chemical calculations [14–16]. Theoretical calculations have been shown a very useful tool for studying the mechanism [17–19].

In the present study, we report the synthesis and structural characterization of tétradentâte symmetrical Schiff bases (Scheme 1). A detailed study of their inhibition behavior, as well as a study on their EIS, polarization curves and weight loss is also reported.

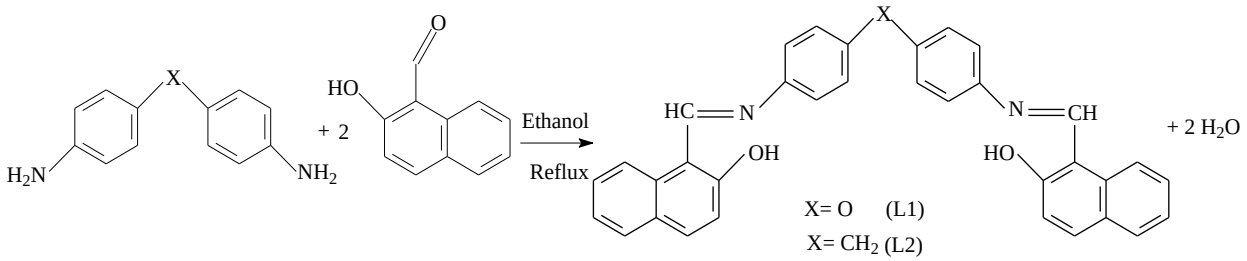

L1: X= O (4,4'-bis(2-hydroxy-1-naphthaldehyde imine)diphenyl ether; $C_{34}H_{24}N_2O_3$)
L2: X= CH_2 (4,4'-bis (2-hydroxy-1-naphthaldéhyde imine)diphenyl methane; $C_{35}H_{26}N_2O_2$)

Scheme 1. Synthetic way for ligands L1 and L2

2. EXPERIMENTAL PROCEDURE

All materials and solvents were analytical reagent grade. 4,4'-diaminodiphenyl ether, 4,4'-diaminodiphenyl methane and 2-Hydroxy-1-naphtaldéhyde were commercial samples supplied by Aldrich and purified by standard procedures. Their purity was determined by thin layer chromatography (TLC).

A three-electrode cell, consisting of carbon steel X48 working electrode (WE) was prepared from a cylindrical carbon steel bar with chemical composition reported as C: 0.45-0.50, Si ≤ 0.40, Mn: 0.50-0.80, S: 0.015-0.035, Cr + Ni + Mo ≤ 0.63 and Fe: rest (in wt. %). The electrode was sealed in a Teflon tube with polyester leaving only the working area exposed and so only, its cross section (6 mm in diameter) was allowed to contact the acidic solution. The exposed surface (0.28 cm^2) was polished using different grades of emery paper (800, 1000, 1200, 1500, 2000, 2400 and 4000 graduates) prior to

each experiment, and then rinsed with double distilled water and finally degreased with acetone before their immersion in the acid solution. A counter electrode (CE) was a large plate of platinum (2 cm^2) and the saturated calomel electrode (SCE) was also employed as a reference electrode (RE). All experiments were achieved in room condition without stirring.

2.1. Synthesis of inhibitors

The Schiff bases (Scheme 1) were prepared according to the described procedure [20]. To a stirred ethanoic solution (20 ml) of 4,4'-diaminodiphenyl ether (0.7 g, 1 mmol, MP: 188-192°C) or 4,4'-diaminodiphenyl methane (1.0 g, 1 mmol, MP: 92°C) with 2-Hydroxy-1-naphtaldéhyde (1.75 g, 2 mmol) was added. The light brown solution was stirred and heated to reflux for 3h. A yellow precipitate was obtained that was filtered off and washed with hot ethanol. Yield of products were obtained 88.8% and 80.70% and their melting points 117.59 °C and 256.95°C respectively. Identification of structure of synthesized Schiff bases was performed by IR, DSC and elementary analysis. Elemental analysis calculated for $C_{34}H_{24}N_2O_3$ (L1): calculated: C, 79.77; H, 5.02; N, 5.64. Found: C, 79.41; H, 5.01; N, 5.47% and for $C_{35}H_{26}N_2O_2$ (L2): calculated: C, 82.94; H, 5.34; N, 5.36. Found C, 82.74; H, 5.32; N, 5.29%. FT-IR (KBr, cm^{-1}): ν (C=N) peak at 1622 cm^{-1} (L1) and 1626 cm^{-1} (L2), the absence of a ν(C=O) peak at around 1700 cm^{-1} is symbolic of Schiff's bases condensation, peak of phenolic OH at 3442 cm^{-1} and 3445 cm^{-1} for two compounds respectively. ν = 1242 cm^{-1} (C–O–C).

2.2. Electrolyte

All tests were performed at room temperature. M in 1M HCl. The solutions were prepared by the dilution of analytical grade of 37 % HCl with double distilled water in the absence and presence of inhibitors.

2.3. Weight loss measurements

The weight loss experiments were performed using cylindrical carbon steel coupons (Good fellow, 99.998%) having the dimensions, 2 cm× 2 cm × 0.5 cm, and the exposed total area is 8,058 cm^2. The specimens were scraped with a series of emery paper (100, 220, 320, 800, 1000, 1200, 1500, 2000, 2400 and 4000 grades). The specimens were immersed in 50 mL of 1M HCl with and without the addition of the inhibitor; all the aggressive acid solutions were open to air. After immersion times, the specimens were taken out, washed, dried, and weighed accurately. All weight-loss measurements were performed in triplicates and the maximum standard deviation in the observed weight loss was ±0.1 mg. The loss in weight (mg cm^{-2}), the corrosion rate (mg cm^{-2} h^{-1}) and the percentage of the inhibition efficiency over the exposure time were calculated as reported in our previous work. The average weight loss ΔW(mg) was calculated using the following equation [21]:

$$\Delta W = W_0 - W \quad (1)$$

where W_0 and W are the average weight of specimens before and after immersion, respectively.

The corrosion rate, C_R (mg cm^{-2} h^{-1}) was calculated using the following equation [22]:

$$C_R = \frac{\Delta W}{St} \quad (2)$$

where ΔW is the mass loss, S the area of the specimen (cm^2) and t is the immersion period (h). The percentage inhibition efficiency IE (%) was calculated using the relationship [23]:

$$IE\ (\%) = \left(\frac{C_R - C_{R(inh)}}{C_R}\right) \times 100 \quad (3)$$

C_R and $C_{R(inh)}$ are corrosion rates in the absence and presence of inhibitor, respectively and surface coverage (θ) values were calculated with the following equation:

$$\theta = \left(\frac{C_R - C_{R(inh)}}{C_R}\right) \quad (4)$$

2.4. Electrochemical measurements

Electrochemical experiments were performed using a Voltalab potentiostat model PGZ-301. In order to obtain a steady state open circuit potential, the working electrode was submerged in the aggressive media for 30 min before the measurements. The electrochemical impedance spectroscopy measurements were carried out at open corrosion potential (E_{corr}) with a frequency range within the limits 100 kHz and 10 mHz with a sinusoidal signal amplitude equal to 10 mV. Potentiodynamic anodic and cathodic polarization curves were performed using a scan rate equal 0.5 mV s^{-1} from -250 to -850 mV of anodic or cathodic over potential, respectively for various concentrations of inhibitors.

2.5. Spectroscopiques analysis

IR spectra were registered as KBr discs using a Perkin-Elmer FT-IR 1000 series spectrophotometer in the range 4000-400 cm^{-1}. The melting points were specified with a Kofler bench. The thermograms of DSC were registered on a DSC822e-Mettler-Toledo Software star device in the temperature range from 40 to 400 °C at a rate of 5 °C min^{-1} under a nitrogen purge.

2.6. Scanning electron microscope analysis (SEM)

The carbon steel specimens were scraped with a series of emery paper (100, 320, 800, 1000, 1200, 1500, 2000 and 2400 grade) and then cleaned with distilled water and acetone. After immersion in 1M HCl solution in the absence and the presence of 5×10^{-5} M of inhibitors L1 and L2 at atmosphere conditions for 24 h, the specimen was washed with bidistilled water, dried with a cold air, and then the SEM pictures were registered using JEOL JSM-7001F-Japan. Analytical scanning electron microscope in the vacuum mode by the instrument operated at 10 kV.

2.7.1. Theoretical study

2.7.1. Quantum chemical calculations Study

Quantum chemical study was performed on Schiff bases to esteem the energy of the highest occupied molecular orbital (E_{HOMO}), the lowest unoccupied molecular orbital (E_{LUMO}), the number of transferred electrons (ΔN) and the dipole moment (μ). The calculations were conducted using the Gaussian 09 program and the Gauss View Molecular Visualization program [24]. Geometry optimization of the studied products were carried out by density functional theory (DFT) level with the non-local hybrid density functional B3LYP [25] at basis sets 6-31G (d,p) [26].

2.7.2. Molecular dynamics (MD) simulation

Molecular dynamics simulations were achieved by using Materials Studio 7.0 software from Accelrys Inc. [27]. Fe (1 1 0) plane was cleaved from pure Fe crystal, and then was extended to construct a suitable supercell (10× 10) to obtain the Fe (1 1 0) model with 24.82 Å × 24.82 Å × 10.135 Å. The optimized inhibitor molecule was too built. The MD simulation of the interaction between the inhibitors molecules and the Fe surface (1 1 0) was performed in a simulation box (24.82 Å × 24.82 Å × 25.13 Å) with periodic boundary conditions to model a representative face of an interface deprived of any arbitrary boundary effects. The box includes of a Fe plate and a vacuum layer of 10 Å in height.

3. RESULTS AND DISCUSSION

3.1. Weight loss tests

Table 1. Corrosion parameters obtained by weight-loss test in 1M HCl solution at various concentrations of the tested compounds.

t (h)	compound	C_{inh} (M)	ΔW (g)	C_R (mg cm^{-2} h^{-1})	*IE* (%)
6	L1	Blank	0.073	1.5099	------
		5×10^{-6}	0.039	0.8066	46.58
		7.5×10^{-6}	0.035	0.7239	52.05
		10^{-5}	0.032	0.6619	56.16
		5×10^{-5}	0.028	0.5791	61.64
	L2	Blank	0.0585	1.2099	------
		5×10^{-6}	0.0474	0.9803	18.97
		7.5×10^{-6}	0.0348	0.7197	40.52
		10^{-5}	0.0217	0.4488	62.90
		5×10^{-5}	0.0173	0.3516	70.93
24	L1	Blank	0.189	0.9773	------
		5×10^{-6}	0.082	0.4240	56.61
		7.5×10^{-6}	0.076	0.3930	59.78
		10^{-5}	0.072	0.3723	61.90
		5×10^{-5}	0.049	0.2534	74.07
	L2	Blank	0.1212	0.6266	------
		5×10^{-6}	0.0697	0.3604	42.48
		7.5×10^{-6}	0.0615	0.3180	49.25
		10^{-5}	0.0419	0.2167	65.42

	5×10^{-5}	0.0270	0.1396	77.72

The weight loss of carbon steel specimens in 1M HCl solution, with and without different concentrations of the investigated inhibitors, was determined after different immersion time intervals of 6 and 24 h at room temperature. The Inhibitory efficiency percentage values *IE* (%) and corrosion rate (C_R) found from weight loss method at different concentrations of each inhibitor are given in Table 1.

It has been obtained that the inhibition efficiency of the examined compounds increases with increase in concentration. The maximum inhibition efficiency for each compound was obtained at 5×10^{-5} M and further increase in concentration did not cause any appreciable change in the performance of inhibitors.

It is clear that the gradual increase of the inhibitor concentration from 10^{-6} to 10^{-4} M by weight increases the adsorbed molecules onto the steel surface, which rises the surface coverage and inhibitory efficiency of the examined inhibitors. This impact may be attributed to the accumulation of the inhibitor molecules onto the metal surface, which decreases the interaction between the acidic medium and the metal surface. It can be concluded that these inhibitors act by adsorption on the surface of the carbon steel and the formation of a barrier layer between the metal and the aggressive medium [28].

3.2. Electrochemical impedance spectroscopy

The impedance experiment is a real tool and has been widely used in examining corrosion inhibition processes. It delivers information on both the resistive and capacitive behavior at the interface and makes possible to estimate the performance of the tested compounds as possible inhibitors against metals corrosion [29]. Nyquist representations of the inhibitors are presented in Fig. 1. It is clear from all diagrams that the impedance response of carbon steel in test solution was significantly changed after the addition of the inhibitors. The charge transfer resistance values were found from the diameter of the semicircles of the Nyquist plots. The inhibition efficiency of the inhibitor was calculated from the charge transfer resistance values by the following equation [30]:

$$IE\ (\%) = \left(\frac{R_{ct(inh)} - R_{ct}}{R_{ct(inh)}}\right) \times 100 \quad (5)$$

where R_{ct} and $R_{ct(inh)}$ are the charge transfer resistances of the electrode without and with inhibitor, respectively.

The double layer capacitance (C_{dl}) values were obtained at the f ($-Zi_{max}$) frequency, at which the imaginary component of the impedance is maximal according to equation (6).

$$C_{dt} = \left(\frac{1}{2\pi f(-Zi_{max})}\right) \times \frac{1}{R_{ct}} \quad (6)$$

The values of this calculated *IE* (%) are listed in Table 2 from which it is also seen that the value of *IE* (%) increases as the concentrations of inhibitors increases in the solution.

Table 2. Electrochemical impedance parameters for carbon steel in 1M HCl with and without addition of various concentrations of Schiff bases inhibitors at 25 °C.

Compound	C_{inh} (M)	R_{ct} (Ω cm^2)	C_{dl} (μF cm^{-2})	*IE* (%)	θ
	Blank	20.3232	1054	-	-
L1	2.5×10^{-6}	23.9042	813.5	14.98	0.149
	5×10^{-6}	34.1000	810.6	40.40	0.404
	7.5×10^{-6}	44.8135	704.7	54.61	0.546
	10^{-5}	49.9810	280.0	59.33	0.593
	2.5×10^{-5}	73.3655	214.6	72.29	0.723
	5×10^{-5}	142.3166	139.9	85.21	0.852
L2	2.5×10^{-6}	46.0731	535.8	55.88	0.558
	5×10^{-6}	63.6952	504.5	68.09	0.681
	7.5×10^{-6}	68.3607	461.1	70.27	0.703
	10^{-5}	105.4814	375.3	80.73	0.807
	2.5×10^{-5}	184.4378	214.6	88.98	0.889
	5×10^{-5}	207.0002	135.1	90.18	0.902

The EIS studies (Fig. 1) show that the presence of Schiff bases (0.05 mM) increases the corrosion inhibitors efficiency to 90 % in the corrosive medium.

After analysis of impedance results, we found that the values of the charge transfer resistance, R_{ct}, increases in the inhibitory system than the uninhibited system. A great resistance is associated with the slowing corrosion system and decreases the active surface needed for the corrosion reaction [31], the decrease of C_{dl} with inhibitor concentration is maybe due to a decrease in local dielectric constant and/or an increase in the thickness of a protective layer at the electrode surface [32,33].

The impedance data of carbon steel in 1M HCl are analyzed in terms of an equivalent circuit model (Fig. 2) which R_{ct} is the charge transfer resistance is placed in parallel to the double layer capacitance C_{dl} both in series with the solution resistance R_S.

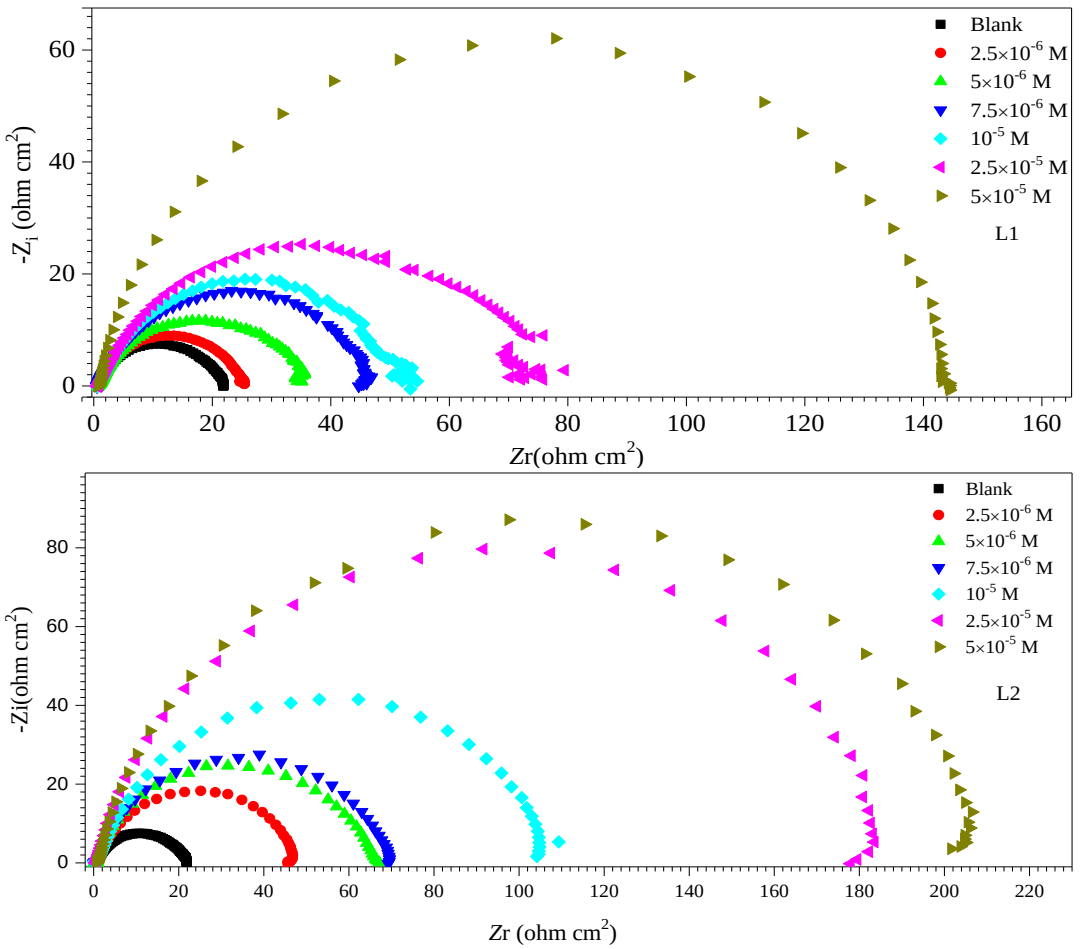

Figure 1. Nyquist diagrams for carbon steel in 1M HCl containing different concentrations of Schiff bases inhibitors at room temperature.

Figure 2. The equivalent circuit model used to fit the experimental results.

3.3. Tafel polarization

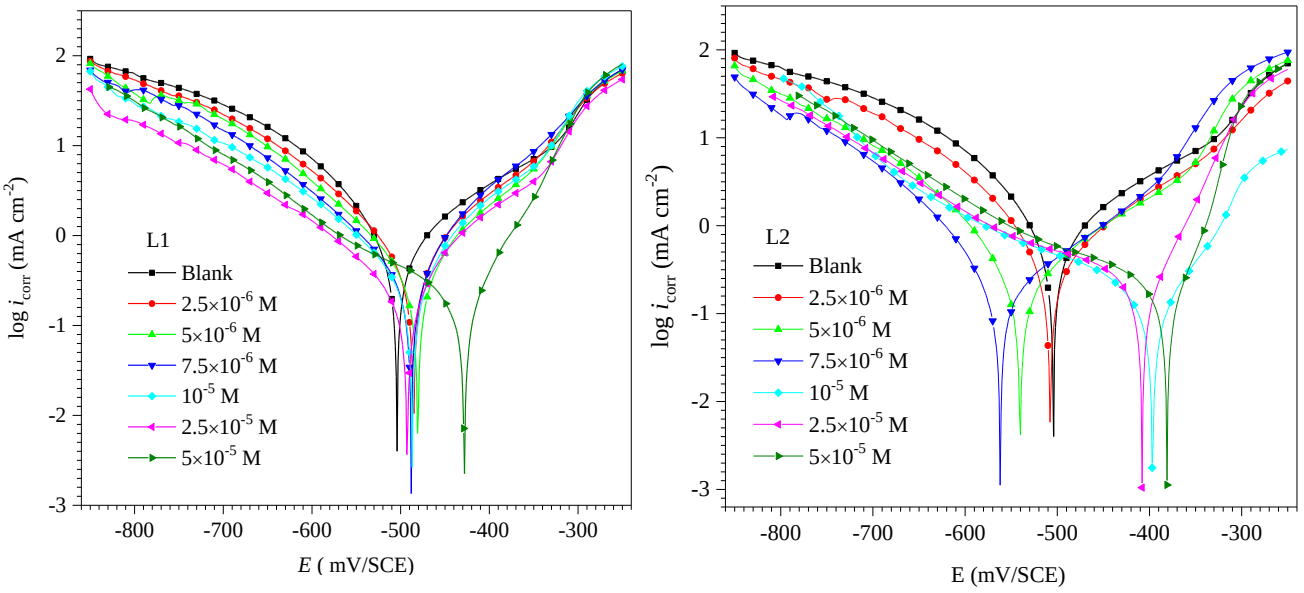

Figure 3. Tafel polarization curves for carbon steel obtained at 25 °C in 1M HCl solution containing various concentrations of inhibitors.

Fig. 3 shows anodic and cathodic polarization plots recorded on a carbon steel electrode in 1M HCl in the absence and presence of different concentrations of inhibitors at ambient temperature. Corrosion is an electrochemical phenomenon and inhibitors decrease the velocity of electrochemical electrode reactions. Table 3 shows the electrochemical corrosion kinetic parameters, i.e., corrosion potential (E_{corr}), cathodic and anodic Tafel slopes (β_c, β_a) and corrosion current density (i_{corr}) found by extrapolation of the Tafel lines.

E_{corr} values of inhibited and uninhibited systems do not vary significantly, which indicate that the addition of the examined compounds affected both anodic and cathodic reactions signifying that the Schiff bases were a mixed kind (anodic/cathodic) inhibitor [34,35]. In each diagram, it is clear that the current density of the anodic and cathodic slops is moved towards inferior values, which indicates the corrosion mitigation. This displacement is more evident with the rise in the concentration of the corrosion inhibitor when compared to the blank material [36]. This result suggests that the addition of the synthesized inhibitors reduces anodic dissolution and retards the hydrogen evolution reaction [37].

The inhibition efficiency *IE* (%) and surface coverage (θ) have been calculated according to equations (7) and (8) respectively [38,39]:

$$IE\ (\%) = \left(\frac{i_{corr} - i_{corr(inh)}}{i_{corr}}\right) \times 100 \quad (7)$$

$$\theta = \left(\frac{i_{corr} - i_{corr(inh)}}{i_{corr}}\right) \quad (8)$$

where $i_{corr(inh)}$ is the inhibited and i_{corr} the inhibited current density, respectively.

It can be seen that the corrosion rate reduced and inhibition efficiency *IE* (%) increased by increasing inhibitor concentration.

Table 3. Corrosion parameters for carbon steel in 1M HCl found by Tafel plots in the absence and presence of the evaluated inhibitors at 25 °C.

Com.	C_{inh} (M)	$-E_{corr}$ (mV/SCE)	$-\beta_c$ (mV/dec)	β_a (mV/dec)	i_{corr} (μA cm^{-2})	R_{ct} (Ω cm^2)	*IE* (%)	θ
	Blank	505	86.9	133.7	650.9	30.91	-	-
	2.5×10^{-6}	503	109.5	106.3	490.2	41.92	24.68	0.25
	5×10^{-6}	509	114.5	101.7	370.8	54.17	43.03	0.43
L1	7.5×10^{-6}	524.5	116.6	82.6	342.8	54.42	47.33	0.47
	10^{-5}	503	118.9	86.3	304.5	63.47	53.21	0.53
	2.5×10^{-5}	530.5	128.4	89.1	215.8	86.45	66.84	0.67
	5×10^{-5}	509	164.7	67.2	173.8	95.73	73.29	0.73
	2.5×10^{-6}	502	82.2	122.5	326.5	53.39	49.83	0.50
	5×10^{-6}	542	89.9	141.4	230.1	88.48	64.64	0.65
L2	7.5×10^{-6}	541	87.3	169.7	207.9	104.8	68.05	0.68
	10^{-5}	525	77.4	131.8	126.7	149.8	80.53	0.81
	2.5×10^{-5}	502.5	81.9	48.3	111.9	156.09	82.80	0.83
	5×10^{-5}	496	62.7	76.5	76.5	169.5	88.24	0.88

3.4. Adsorption isotherm

The adsorption isotherm can deliver significant information about the interaction of the Schiff base products and the metal surface, so it is essential to know the mode of adsorption (chemisorption or physisorption), and the adsorption isotherm that fits the experimental data. Langmuir adsorption isotherm was found to provide the top description of the adsorption behavior of the examined inhibitors [40,41]. A straight line is obtained by plotting C/θ *vs.* C for L1 and L2 as presented in Fig. 4. The regression coefficients of the fitted curves are around unity (R^2 = 0.999 for L1 and R^2 = 0.994 for L2), demonstrating that the adsorption of these inhibitors on the carbon steel surface obeys the Langmuir isotherm which is given by the following equation [42]:

$$\frac{C}{\theta} = \frac{1}{K_{ads}} + C_{inh} \quad (9)$$

where K_{ads} is the equilibrium constant of the adsorption process equal to 1.53×10^5 M^{-1} and 6.76×10^5 M^{-1} for L1 and L2, respectively.

K_{ads} is related to the standard Gibbs free energy of adsorption, ΔG^0_{ads} according to [43].

$$\Delta G^0_{ads} = -RT \ln (55.5\, K_{ads}) \quad (10)$$

where R (J mol^{-1} K^{-1}) is the universal gas constant and T (K) is the absolute temperature and 55.5 (mol L^{-1}) is the molar concentration of water in solution.

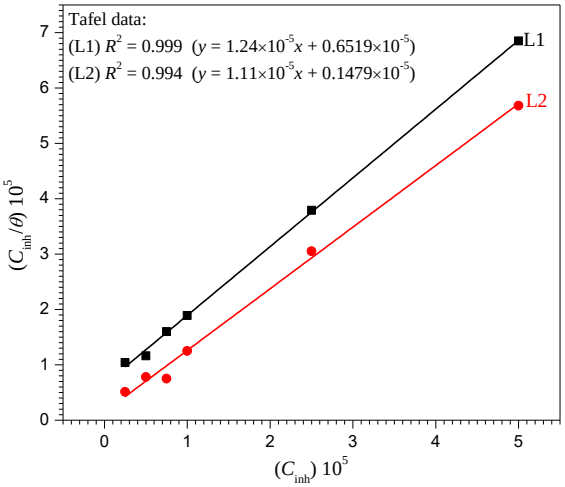

Figure 4. Langmuir adsorption plots for carbon steel in HCl 1M containing different concentrations of Schiff bases compounds

From Eq. (10), the value of ΔG^0_{ads} was calculated as -39.52 KJ mol^{-1} and -43.19 kJ mol^{-1}. The negative values of ΔG^0_{ads} designate spontaneous adsorption of molecules on the carbon steel surface and strong interaction between inhibitor molecules and the metal surface. It is established that the values of ΔG^0_{ads}around or less than -20 kJ mol^{-1} indicate physisorption and the values of ΔG^0_{ads} around or greater than -40 kJ mol^{-1} are considered as chemisorption. This indicated that the adsorption of investigated Schiff bases on the metal surface is chemisorption [44].

3.5. Scanning electron microscopic (SEM) analysis

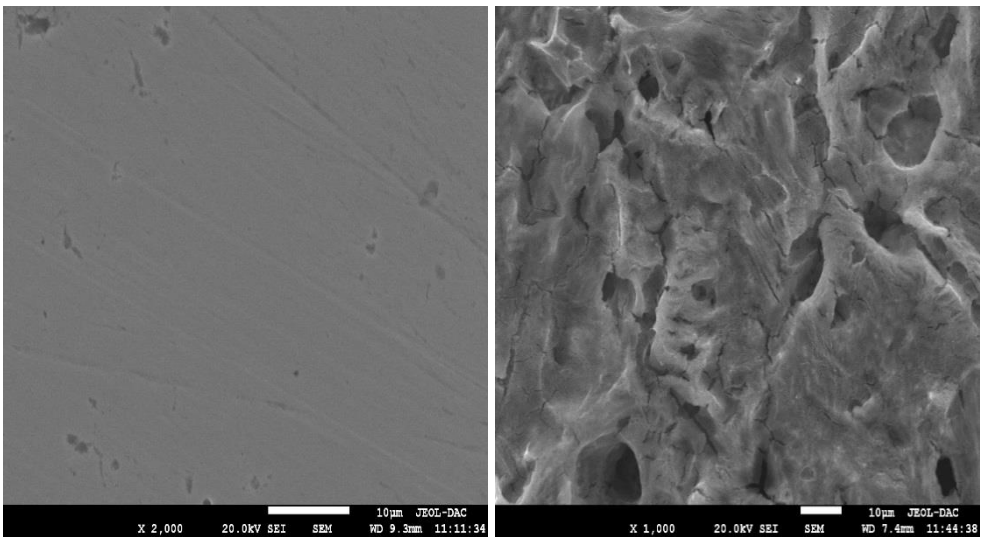

(a) **(b)**

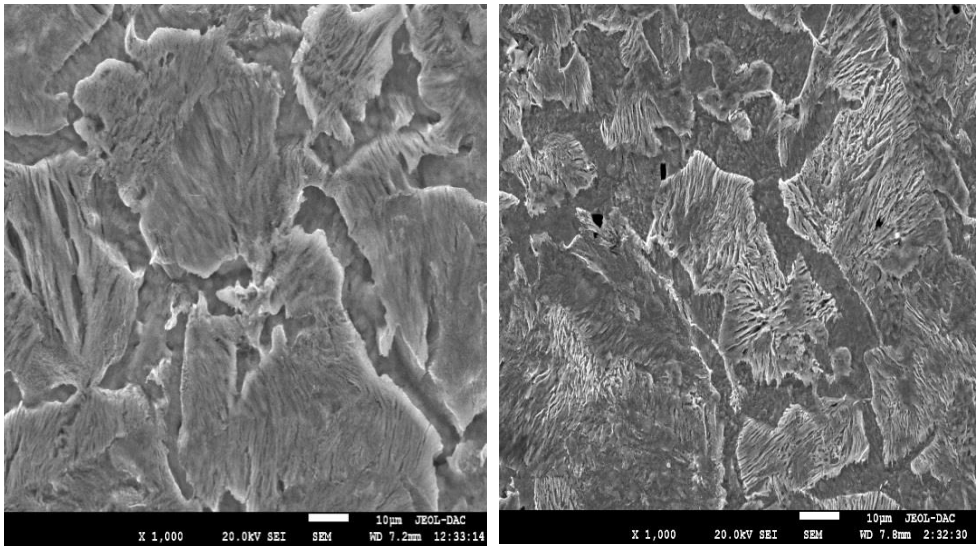

(c) **(d)**

Figure 5. SEM pictures of: (a) freshly polished carbon steel surface abraded without immersion in test solutions at 25 °C, (b) after 24 h immersion in 1M HCl without inhibitor, (c) after 24 h immersion in 1M HCl containing 5×10^{-5} M of the inhibitor L1 and, (d) after 24 h immersion in 1 M HCl containing 5×10^{-5} M of the inhibitor L2.

The surface images of the carbon steel exposed to 1M HCl in the absence and presence of Schiff bases were obtained by SEM. The experimental results were gathered (Fig. 5), from which it can be seen that before immersion, the metal surface seemed smooth (Fig. 5a). In the presence of the uninhibited 1M HCl solution, a damaged and heterogeneous surface is observed because of severe corrosion of carbon steel by the aggressive acid (Fig. 5b). However, in the presence of the inhibitors L1 and L2 (Fig. 5c and d) respectively, much less damage was caused on the metal surface, which confirms the inhibition effect. Therefore, it can be concluded that the Schiff bases possess a good inhibiting ability for steel corrosion [45,46].

3.6. Theoretical section

3.6.1. DFT calculation

The inhibitory effect of the inhibitors regularly depends on the adsorption of these molecules on the metal surface, this adsorption depending on the molecular structures [47]. Amongst quantum chemical approaches for evaluation of corrosion inhibitors, density functional theory (DFT) has some merits and appears to be adequate for obtaining the required electronic data responsible for inhibitory action [48]. The frontier orbitals electron density distributions have a great importance in describing the adsorption preference of the inhibitors [49]. The reactive ability of the inhibitor is considered to be closely related to their frontier molecular orbitals, the HOMO and LUMO [50,51]. The following quantum chemical indices were considered: the energy of the highest occupied molecular orbital (E_{HOMO}), the energy of the lowest unoccupied molecular orbital (E_{LUMO}), $\Delta E = E_{LUMO}$-E_{HOMO} and the dipole moment (μ). The E_{HOMO} is often associated with the electron donating ability of a molecule. The inhibition efficiency increases with increasing E_{HOMO}, values. High E_{HOMO} values indicate that the

molecule has a tendency to donate electrons to appropriate acceptor molecules with low energy empty molecular orbitals. E_{LUMO} indicates the ability of the molecule to accept electrons. The lower value of E_{LUMO}, suggesting that the molecule easily accepts electrons from the donor molecules [52]. The calculated parameters of the two molecules such as E_{HOMO}, E_{LUMO}, ΔE_{gap}= E_{LUMO}-E_{HOMO} and the dipole moment (μ), the Ionization Potential (I), the Electron Affinity (A), the electronegativity (χ), the global hardness (η), the global softness (σ), and the fraction of electron transferred (ΔN) are shown in Table 4. The ionization potential (I) and the electron affinity (A) are defined as follows:

$$I = -E_{HOMO} \quad (11)$$

$$A = -E_{LUMO} \quad (12)$$

Then the electronegativity and the global hardness were evaluated, based on the finite difference approximation, as linear combinations of the calculated I and A [49].

$$\chi = \frac{I+A}{2} \quad (13)$$

$$\eta = \frac{I-A}{2} \text{ (eV)} \quad (14)$$

Softness is the inverse of hardness:

$$\sigma = \frac{1}{\eta} \quad (15)$$

The obtained values of χ and η are used to calculate the fraction of the electron transferred, ΔN, from the inhibitor to metallic surface as follow [53]:

$$\Delta N = \frac{\chi_{Fe} - \chi_{inh}}{2(\eta_{Fe} + \eta_{inh})} \quad (16)$$

In order to calculate the fraction of electrons transferred, a theoretical value for the electronegativity of iron was employed χ_{Fe} = 7 eV and a global hardness of η_{Fe}= 0 eV [54].

The optimized structures of the examined Schiff bases in the neutral form including their HOMO and LUMO distributions density are presented in Figs. 6, 7 and 8. Positive and negative regions are shown by green and red colors respectively.

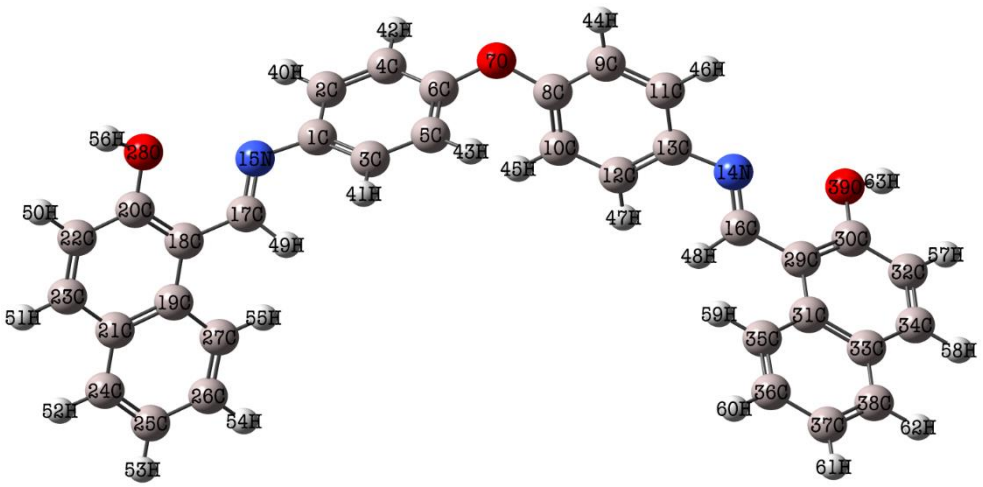

(L1)

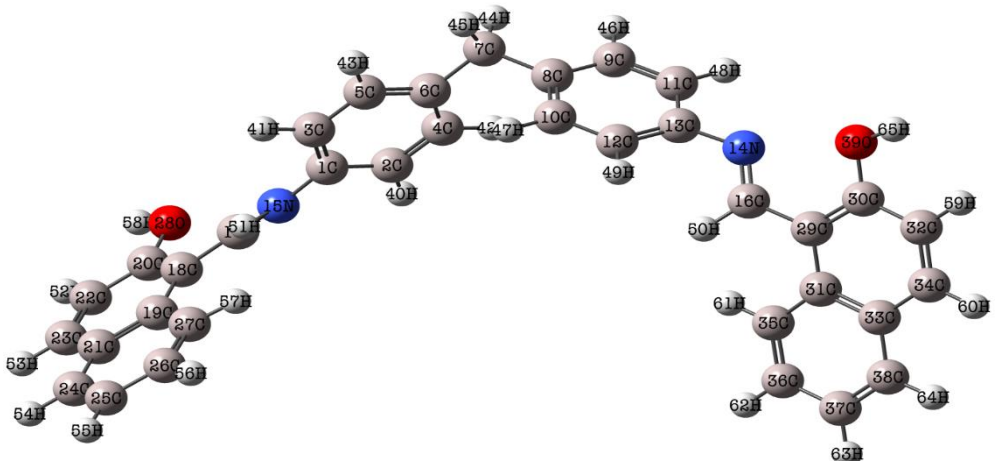

(L2)

Figure 6. Optimized molecular structures of L1 and L2.

Chemical reactivity and kinetic stability of the molecule are designated by the Frontier orbitals. A large HOMO–LUMO gap implies high kinetic stability and low chemical reactivity, as it is energetically unfavorable to add an electron to a high-lying LUMO, to extract electrons from low-lying HOMO.

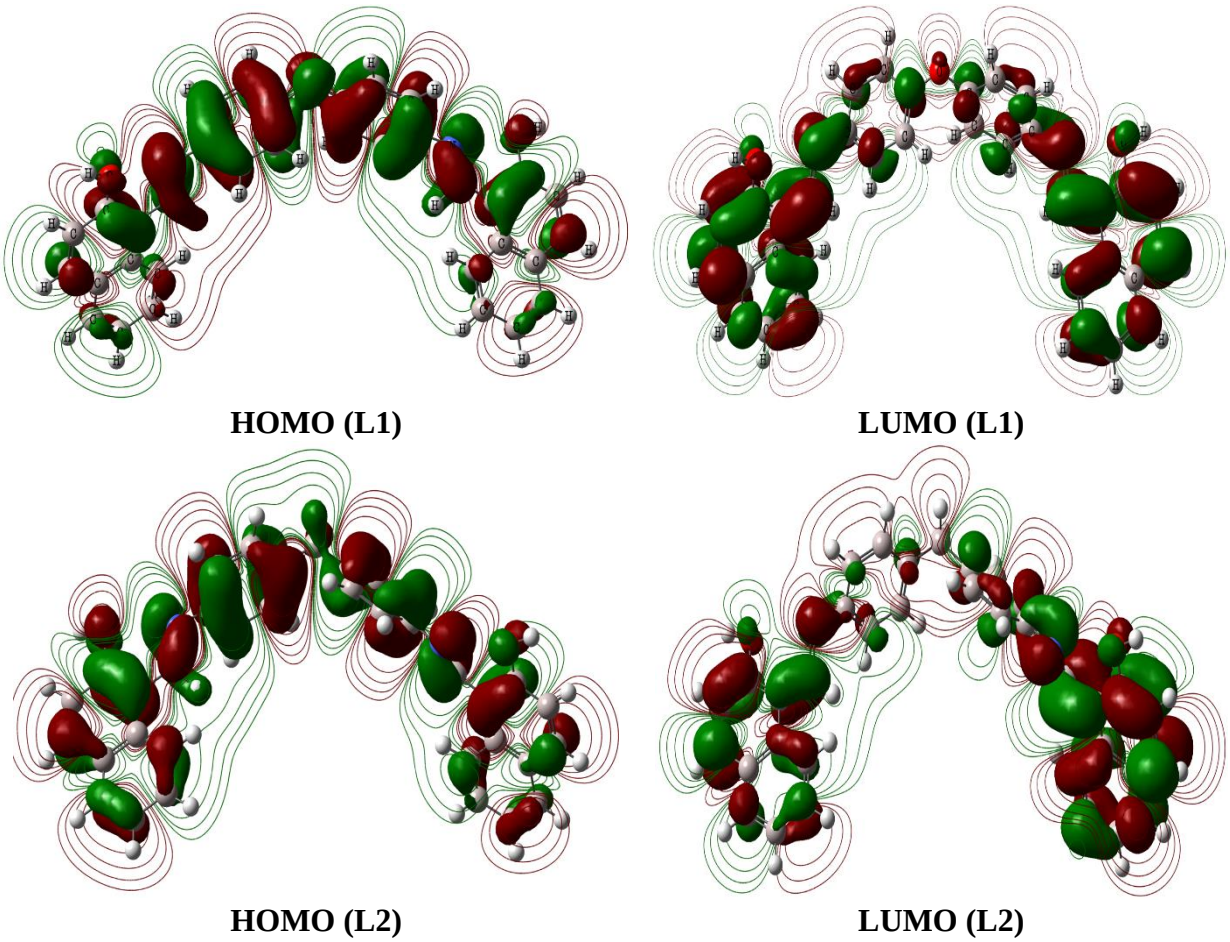

HOMO (L1) **LUMO (L1)**

HOMO (L2) **LUMO (L2)**

Figure 7. Frontier molecule orbital density distributions of L1 and L2: HOMO (left); LUMO (right).using DFT at the B3LYP/6-31G (d,p) basis set level.

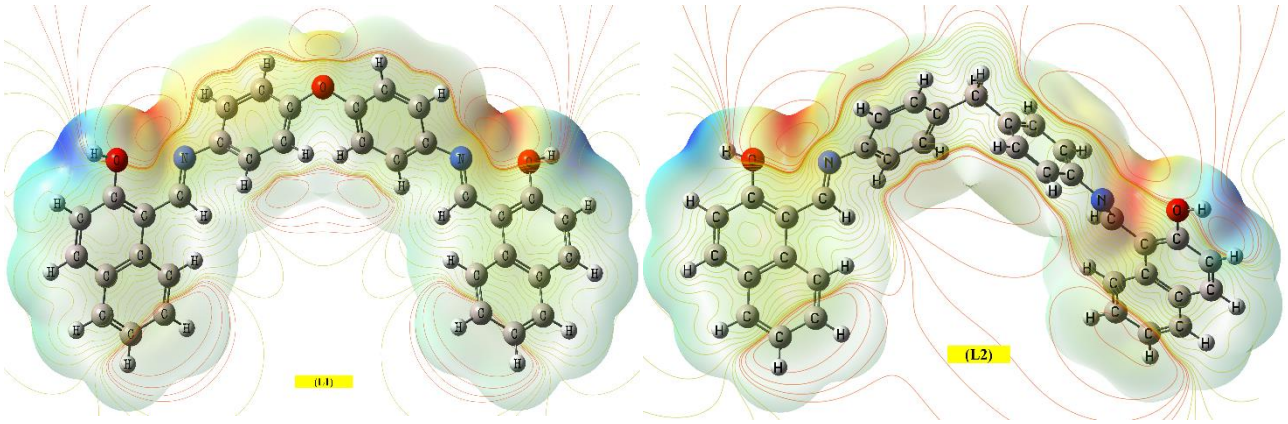

Figure 8. Contour map of electrostatic potential calculated by the DFT/B3LYP//6-31G (d,p) of L1 and L2 inhibitors.

The energy difference between the HOMO and LUMO are -7.22 and -7.10 eV for L1 and L2, respectively, which implies that the compound L2 has a higher kinetic stability and high inhibition efficiency.The dipole moment (μ) is a measure of the polarity of a covalent bond, which is related to the distribution of electrons in a molecule, the low value of dipole moment of the molecule may decrease the dipole–dipole interaction [55]. The values of the dipole moment of L1 and L2 are 3.89 and 2.71 Debye, respectively, suggesting that L2 molecules are more favored for the accumulation of the inhibitor molecules on the metal surface. The fraction of electrons transferred (ΔN) values describes the inhibition achieved from electron donations. The inhibition efficiency increases with increasing electron-donation ability to the metal surface [56].

Table 4. Quantum parameters of two compounds calculated using DFT at the B3LYP/6-31G (d,p) basis set.

Quantum parameter	E_{HOMO} (eV)	E_{LUMO} (eV)	ΔE (eV)	μ (D)	I (eV)	A (eV)	χ (eV)	η (eV)	σ	ΔN (eV)
L1	-6.30	0.92	7.22	3.89	6.30	-0.92	2.69	3.61	0.27	0.59
L2	-6.17	0.93	7.10	2.71	6.17	-0.93	2.62	3.55	0.28	0.61

Mulliken charge analysis is used to estimate the adsorption centers of inhibitors, the calculated Mulliken charges of selected atoms are presented in Table 5. It is possible to observe that the heteroatom afford a noticeable excess of negative charges could act as a nucleophilic reagent [57]. Therefore, are the active adsorption sites. The highest negative charges were located on O7 (-0.57) and N14 (-0.456) atoms, and negative charges around carbon atoms of the aromatic rings. Natural bonding orbital (NBO) analysis is performed to understand intramolecular bonding and interaction among bonds [58], NBO examination is used to calculate the distribution of electron density in atoms and in bonds between atoms, the negative NBO charges were detected on O7, C7, N14, O28 and O39 atoms

for both molecules. The highest negative charge was detected on O39 as (-0.65833) and (-0.65819) for L1 and L2, respectively. NBO values are listed in Table 5.

Table 5. Mulliken and NBO atomic charges for L1 and L2 molecules.

L1			L2		
Atom	Mulliken charges	NBO charges	Atom	Mulliken charges	NBO charges
C1	0.239778	0.12833	C1	0.247938	0.11585
C2	-0.095713	-0.22556	C2	-0.104502	-0.21826
C3	-0.096188	-0.26019	C3	-0.108730	-0.25165
C4	-0.124397	-0.22507	C4	-0.124518	-0.27037
C5	-0.153305	-0.23034	C5	-0.121925	-0.28793
C6	0.137479	-0.03909	C6	0.320050	0.29697
C7	-0.309531	-0.48380	O7	-0.575284	-0.50964
C8	0.136375	-0.03968	C8	0.320042	0.29696
C9	-0.145713	-0.23296	C9	-0.124516	-0.27037
C10	-0.130595	-0.22169	C10	-0.121915	-0.28792
C11	-0.093918	-0.22648	C11	-0.104505	-0.21827
C12	-0.097180	-0.25820	C12	-0.108731	-0.25166
C13	0.240411	0.12831	C13	0.247936	0.11585
N14	-0.453806	-0.41728	N14	-0.456486	-0.41801
N15	-0.452344	-0.41653	N15	-0.456470	-0.41801
C16	0.088042	0.09301	C16	0.087207	0.09116
C17	0.088196	0.09306	C17	0.087179	0.09115
C18	0.043252	-0.14349	C18	0.043563	-0.14318
C19	0.049782	-0.01769	C19	0.049997	-0.01790
C20	0.283017	0.37402	C20	0.282916	0.37372
C21	0.100045	-0.07704	C21	0.099943	-0.07695
C22	-0.126367	-0.30562	C22	-0.126349	-0.30547
C23	-0.131031	-0.17979	C23	-0.131105	-0.17994
C24	-0.130325	-0.20297	C24	-0.130202	-0.20281
C25	-0.092698	-0.24717	C25	-0.092739	-0.24715
C26	-0.091754	-0.22344	C26	-0.091652	-0.22348
C27	-0.138763	-0.22835	C27	-0.138693	-0.22851
O28	-0.520241	-0.65797	O28	-0.520649	-0.65834
C29	0.043603	-0.14338	C29	0.043584	-0.14319
C30	0.282523	0.37382	C30	0.282906	0.37373
C31	0.049358	-0.01766	C31	0.049982	-0.01790
C32	-0.126264	-0.30579	C32	-0.126349	-0.30548
C33	0.100195	-0.07707	C33	0.099942	-0.07695
C34	-0.131045	-0.17981	C34	-0.131104	-0.17994
C35	-0.139008	-0.22823	C35	-0.138690	-0.22851
C36	-0.091775	-0.22320	C36	-0.091655	-0.22348
C37	-0.092705	-0.24705	C37	-0.092738	-0.24715
C38	-0.130342	-0.20314	C38	-0.130202	-0.20281
O39	-0.520452	-0.65819	O39	-0.521212	-0.65833

3.6.2. Molecular dynamic simulation

structure top view side view

(**L1**)

(**L2**)

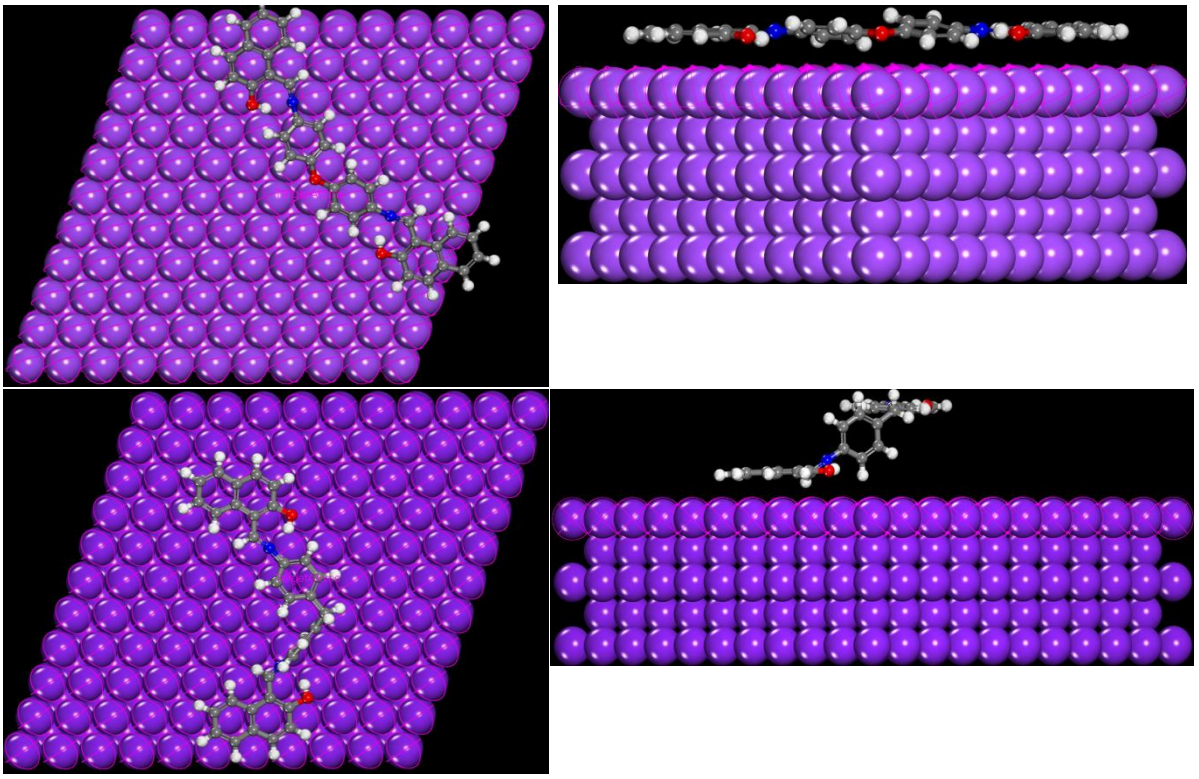

Figure 9. Equilibrium adsorption configurations of inhibitors L1 and L2 on Fe (1 1 0) surface obtained by molecular dynamic simulations.

Molecular dynamics can be applied to the structural study of molecules as well as to large interacting systems. These simulations serve as structural and dynamic models for the comprehension of experimental results. The behavior of the inhibitors on the surface was studied by MD simulations. The use of the molecular dynamics simulations is a useful and modern tool to research the interaction between inhibitors and metal surface [59]. Fig. 9 shows the equilibrium configurations of inhibitor molecules on the Fe (1 1 0) surfaces, the formation of the flat or parallel orientation on steel surface can be attributed to the relatively equal distribution of HOMO and LUMO densities on the whole molecule, confirming the strong interaction between the molecule and iron atoms [60]. The calculated adsorption energy and rigid adsorption energy are presented in Table 6. Large negative values of adsorption energies mean that the interaction between inhibitor molecules and Fe surface is strong and indicates the spontaneity of the adsorption process [61]. The high values of E_{ads} for L2 and L1 reflect the higher stability of inhibitor/surface interaction and accordingly increase their inhibition efficiencies [62,63]. This result is in agreement with the experimentally determined inhibition efficiencies.

Table 6. Outputs and descriptors calculated by the molecular dynamic simulations for adsorption of L1 and L2 derivatives on Fe (1 1 0) surface.

System	Total energy	Adsorption energy	Rigid adsorption energy	Deformation energy
L1-Fe(1 1 0)	-118.25	-454.13	-304.84	-149.29
L2-Fe(1 1 0)	-121.17	-457.19	-301.16	-156.02

4. CONCLUSIONS

The results presented in this work concern the synthesis of new compounds Schiff bases 4,4'-bis(2-hydroxy-1-naphthaldehyde imine)diphenyl ether (L1) and 4,4'-bis(2-hydroxy-1-naphthaldehyde imine) diphenyl methane (L2). Then, the characterization of these compounds by different methods of analysis (DSC, infrared (IR), elementary analysis and the study of these new Schiff bases was investigated on the corrosion of carbon steel XC48 in a 1M hydrochloric acid environment using weight loss, electrochemical impedance spectroscopy and curves of polarization.

- The inhibition efficiency measured through weight loss test can reach about 78 % at 5×10^{-5} M for two Schiff bases.

- Characterization by impedance spectroscopy shows that the charge transfer resistance increases with the increase in inhibitor concentration, while the capacity of the double layer decreases as the quantity of inhibitor increases.

- The results obtained by the plots of the polarization curves show that these Inhibitors are effective against corrosion of XC48 steel in 1M HCl media. We have inhibition efficiency increases with the inhibitor concentrations achieved 73.29 % for L1 and 88.24 % for L2; this study indicated that the tested compounds were of mixed type (cathodic/anodic) inhibitors.

- The results obtained from electrochemical measurements showed that the adsorption of Schiff bases L1 and L2 on carbon steel in 1M HCl solution follows Langmuir isotherm.

- A good agreement between the values of the inhibition efficiency determined by polarization Potentiodynamic (Tafel), by electrochemical impedance spectroscopy (EIS) and by weight loss.

- The SEM images showed the presence of protective film on the carbon steel surface indicating the adsorption of products.

- The quantum chemical methods display a good relationship between the theoretical and experimental electrochemical study.

References

1. M. Hosseini, S.F.L Mertens, M. Ghorbani, M.R. Arshadi, *J. Appl. Electrochem.*, 38 (2003) 1629.
2. Y.A. Balaban, S. Kandemir, G. Bereket, Y. Erk, *Mater. Chem. Phys*., 85 (2004) 420.
3. M. Behpour, S.M. Ghoreishi, M. Salavati-Niasari, B. Ebrahimi, *Mater. Chem. Phys*., 107 (2008) 153.
4. S. Bilgiç, N. Çaliskan, *J. Appl. Electrochem*., 31 (2001) 79.
5. Y.K. Agrawal, J.D. Talati, M.D. Shah, M.N. Desai, N.K. Shah, *Corros. Sci*., 46 (2004) 633.
6. E. Bayol, T. Gurten, A.A. Gurten, M. Erbil, *Mater. Chem. Phys.*, 112 (2008) 624.
7. I.A. Aiad. N.A. Negm, *J. Surfact. Deterg.*, 12 (2009) 313.
8. S. Ilhan, H. Baykara, M.S. Seyitoglu, A. Levent, S. Ozdemir, A. Dundar, A. Oztomsuk, M.H. Cornejo, *J. Mol. Struct*., 1075 (2014) 32.
9. K.M. Govindaraju, D. Gopi, L. Kavitha, *J. Appl. Electrochem*., 39 (2009) 2345.
10. M. Heydari, M. Javidi, *Corros. Sci.*, 61 (2012) 148.
11. X. Jiang, Y.G. Zheng, W. Ke, *Corros. Sci*., 47 (2005) 2636.

12. A. Garnica-Rodriguez, J. Genesca, J. Mendoza-Flores, R. Duran-Romero, *J. Appl. Electrochem.*, 39 (2009) 1809.
13. P.C. Okafor, X. Liu, Y.G. Zheng, *Corros. Sci*., 51 (2009) 761.
14. El Sayed H. El Ashry, Ahmed El Nemra, Sami A. Esawy, Safaa Ragaba, *Electrochim. Acta,* 51 (2006) 3957.
15. P. Zhao, Q. Liang, Y. Li, *Appl. Surf. Sci.,* 252 (2005) 1596.
16. Y. Xiao-Ci, Z. Hong, L. Ming-Dao, R. Hong-Xuang, Y. Lu-An, *Corros. Sci*., 42 (2000) 645.
17. D. Wang, S. Li, Y. Ying, M. Wang, H. Xiao, Z. Chen, *Corros. Sci*., 41 (1999) 1911.
18. G. Bereket, E. Hur, C. Ogretir, *J. Mol. Struct. Theochem,* 578 (2002) 79.
19. C. Ogretir, G. Bereket, *J. Mol. Struct. Theochem,* 488 (1999) 223.
20. Y.P. Cai, C.Y. Su, A.W. Xu, B.S. Kang, Y.E.X. Tong, H.Q. Liu, S. Jie, *Polyhedron,* 20 (2001) 657.
21. A.A. Farag, M.R. Noor El-Din, *Corros. Sci*., 64 (2012) 174.
22. K. Boumhara, F. Bentiss, M. Tabyaoui, J. Costa, J.M. Desjobert, A. Bellaouchou, A. Guenbour, B. Hammouti, S.S. Al-Deyab, *Int. J. Electrochem. Sci*., 9 (2014) 1187.
23. Q.B. Zhang, Y.X. Hua, *Electrochim. Acta,* 54 (2009) 1881.
24. Gaussian 09, Revision A.02, M.J. Frisch, G.W. Trucks, H.B. Schlegel, G.E. Scuseria, M.A. Robb, J.R. Cheeseman, G. Scalmani, V. Barone, G.A. Petersson, H. Nakatsuji, X. Li, M. Caricato, A. Marenich, J. Bloino, B.G. Janesko, R. Gomperts, B. Mennucci, H.P. Hratchian, J.V. Ortiz, A.F. Izmaylov, J.L. Sonnenberg, D. Williams-Young, F. Ding, F. Lipparini, F. Egidi, J. Goings, B. Peng, A. Petrone, T. Henderson, D. Ranasinghe, V. G. Zakrzewski, J. Gao, N. Rega, G. Zheng, W. Liang, M. Hada, M. Ehara, K. Toyota, R. Fukuda, J. Hasegawa, M. Ishida, T. Nakajima, Y. Honda, O. Kitao, H. Nakai, T. Vreven, K. Throssell, J.A. Montgomery, Jr., J.E. Peralta, F. Ogliaro, M. Bearpark, J.J. Heyd, E. Brothers, K.N. Kudin, V.N. Staroverov, T. Keith, R. Kobayashi, J. Normand, K. Raghavachari, A. Rendell, J.C. Burant, S.S. Iyengar, J. Tomasi, M. Cossi, J.M. Millam, M. Klene, C. Adamo, R. Cammi, J.W. Ochterski, R.L. Martin, K. Morokuma, O. Farkas, J.B. Foresman, D.J. Fox, Gaussian, Inc., Wallingford CT, 2016.
25. C. Lee, W. Yang, R.G. Parr, *Phys. Rev., B 37* (1988) 785.
26. G.A. Petersson, A. Bennett, T.G. Tensfeldt, M.A. Al-Laham, W.A. Shirley, J. Mantzaris, *J. Chem. Phys*., 89 (1988) 2193.
27. Materials Studio, version 7.0, Accelrys Inc., San Diego, USA, 2013.
28. I.B. Obot, N.O. Obi-Egbedi, N.W. Odozi, *Corros. Sci*., 52 (2010) 923.
29. F. Bentiss, B. Mernari, M. Traisnel, H. Vezin, M. Lagrenee, *Corros. Sci*., 53 (2011) 487.
30. I. Ahamad, R. Prasad, M.A. Quraishi, *Mater. Chem. Phys*., 124 (2010) 1155.
31. K.R. Ansari, M.A. Quraishi, A. Singh, *Corros. Sci*., 79 (2014) 5.
32. T. Douadi, H. Hamani, D. Daoud, M. Al-Noaimi, S. Chafaa, *J. Taiwan Inst. Chem. E.,* 71 (2017) 388.
33. F. Zhang, Y. Tang, Z. Cao, W. Jing, Z. Wu, Y. Chen, *Corros. Sci*., 61 (2012) 1.
34. K.S. Jacob, G. Parameswaran, *Corros. Sci*., 52 (2010) 224.
35. H. Hamani, T. Douadi, M. Al-Noaimi, S. Issaadi, D. Daoud, S. Chafaa, *Corros. Sci*., 88 (2014) 234.
36. L. Fragoza-Mar, O. Olivares-Xometl, M.A. Domínguez-Aguilar, E.A. Flores, P. Arellanes-Lozada, F. Jiménez-Cruz, *Corros. Sci*., 61 (2012) 171.
37. M.A. Hegazy, *Corros. Sci*., 51 (2009) 2610.
38. H. Hamani, T. Douadi, D. Daoud, M. Al-Noaimi, R. A. Rikkouh, S. Chafaa, *J. Electroanal. Chem*., 801 (2017) 425.
39. A.S. Patel, V.A. Panchal, G.V. Mudaliar, N.K. Shah, *J. Saudi Chem. Soc*., 17 (2013) 53.
40. R. Yildiz, *Corros. Sci*., 90 (2015) 544.
41. S. Benabid, T. Douadi, S. Issaadi, C. Penverne, S. Chafaa, *Measurement,* 99 (2017) 53.
42. H. Hamani, T. Douadi, D. Daoud, M. Al-Noaimi, S. Chafaa, Measurement, 94 (2016) 837.
43. T.P. Zhao, G.N. Mu, *Corros. Sci*., 41 (1999) 1937.
44. K. Ramya, R. Mohan, K.K. Anupama, A. Joseph, Mater. *Chem. Phys*., 149–150 (2015) 632.

45. S. Issaadi, T. Douadi, S. Chafaa, *Appl. Surf. Sci*., 316 (2014) 582.
46. D. Daoud, T. Douadi, H. Hamani, S. Chafaa, M. Al-Noaimi, *Corros. Sci*., 94 (2015) 21.
47. M.K. Awad, M.R. Mustafa, M.M. Abo Elnga, *J. Mol. Struct. Theochem*, 959 (2010) 66.
48. M. Lashkari, M.R. Arshadi, *Chem. Phys*., 299 (2004) 131.
49. D. Daoud1, T. Douadi, H. Hamani, D. Ghobrini1, K. Aiboud, 3rd International Conference on Control, Engineering & Information Technology, CEIT 2015, DOI :10.1109/CEIT.2015.7233032.
50. T. Arslan, F. Kandemirli, E.E. Ebenso, I. Love, H. Alemu, *Corros. Sci*., 51 (2009) 35.
51. A. Zarrouk, B. Hammouti, T. Lakhlifi, M. Traisnel, H. Vezin, F. Bentiss, *Corros. Sci*., 90 (2015) 572.
52. M. Yadav, S. Kumar, D. Behera, I. Bahadur, D. Ramjugernath, *Int. J. Electrochem. Sci*., 9 **(**2014**)** 5235.
53. V.S. Sastri, J.R. Perumareddi, *Corrosion, 53* (1997) 617.
54. L.M. Rodriguez-Valdez, A. Martinez-Villafane, D. Glossman-Mitnik, *J. Mol. Struct. Theochem*, 716 (2005) 61.
55. D. Daoud, T. Douadi, S. Issaadi, S. Chafaa, *Corros. Sci*., 79 (2014) 50.
56. H. Ju, Z.P. Kai, Y. Li, *Corros. Sci*., 50 (2008) 865.
57. G. Gao, C. Liang, *Electrochim. Acta*, 52 (2007) 4554.
58. A.O. Yüce, B.D. Mert, G. Kardaş, B. Yazıcı, *Corros. Sci*., 83 (2014) 310.
59. S. Kaya, L. Guo, C. Kaya, B. Tüzün, I.B. Obot, R. Touir , N. Islam, *J. Taiwan Inst. Chem. E*., 65 (2016) 522.
60. X. Li, X. Xie, S. Deng, G. Du, *Corros. Sci*., 87 (2014) 27.
61. S. Kaya, C. Kaya, L. Guo, F. Kandemirli, B. Tüzün, I. Uğurlu, L.H. Madkour, M. Saraçoğlu, *J. Mol. Liq*., 219 (2016) 497.
62. M.K. Awad, M.R. Mustafa, M.M. Abo Elnga, *J. Mol. Struct. THEOCHEM*, 959 (2010) 66.
63. N. Chafai, S. Chafaa, K. Benbouguerra, D. Daoud, A. Hellal, M. Mehri, *J. Taiwan Inst. Chem. E*., 70 (2017) 331.